Detecting and Locating Boats Using a PTZ Camera with Both Optical and Thermal Sensors

Simonsen, Christoffer Plovmand; Theisson, Frederik Myrup; Holtskog, Øjvind; Gade, Rikke

Published in:
15th International Conference on Computer Vision Theory and Applications

DOI (link to publication from Publisher):
10.5220/0008972603950403

Publication date:
2020

Document Version
Accepted author manuscript, peer reviewed version

Detecting and Locating Boats Using a PTZ Camera with Both Optical and Thermal Sensors

Christoffer P. Simonsen[1][a], Frederik M. Thiesson[1][b] Øyvind Holtskog[1][c] and Rikke Gade[1][d]

[1] *Department of Architecture, Design and Media Technology, Aalborg University, Fredrik Bajers Vej, Aalborg, Denmark*
{cpsi15, fthies15, aholts15}@student.aau.dk, rg@create.aau.dk

Keywords: Object detection, CNN, PTZ camera, Transfer-learning, Thermal camera, Single camera positioning, Ray-casting.

Abstract: A harbor traffic monitoring system is necessary for most ports, yet current systems are often not able to detect and receive information from boats without transponders. In this paper we propose a computer vision based monitoring system utilizing the multi-modal properties of a PTZ (pan, tilt, zoom) camera with both an optical and thermal sensor in order to detect boats in different lighting and weather conditions. In both domains boats are detected using a YOLOv3 network pretrained on the COCO dataset and retrained using transfer-learning to images of boats in the test environment. The boats are then positioned on the water using ray-casting. The system is able to detect boats with an average precision of 95.53% and 96.82% in the optical and thermal domains, respectively. Furthermore, it is also able to detect boats in low optical lighting conditions, without being trained with data from such conditions, with an average precision of 15.05% and 46.05% in the optical and thermal domains, respectively. The position estimator, based on a single camera, is able to determine the position of the boats with a mean error of 18.58 meters and a standard deviation of 17.97 meters.

1 INTRODUCTION

Port traffic management is a crucial operation in large ports and is given much attention throughout the world [Branch, 1986]. The aim of such a system is to use all sources of information in order to build a comprehensive situation awareness [Council of the European Union, 2008]. Current major ports use monitoring systems for large industrial or passenger boats. Well-trained human operators use sophisticated tools at their disposal in order monitor all activity within their area. These tools include: radars, information systems, and a large number of communication tools, which are all aiding the operators in providing information on request and coordinate movement of boats [Wiersma and Mastenbroek, 1998]. However, smaller ports experience traffic from a large variety of vessels, ranging from cargo/cruise ships to small kayaks. The smaller vessels are not necessarily equipped with transponders and are therefore most often overlooked in these monitoring systems. Computer vision based solutions have the potential to overcome the problem of locating vessels with no transponders. With the use of cameras, it is possible to detect and determine the position of boats of almost any size in a port without the use of transponders. However, it is important that the system works in all weather and lighting conditions. Sole use of an optical sensor would likely fail to detect boats in poor lighting conditions, such as during the night or in heavy rain. This leads us to our proposed computer vision based solution.

In this paper we propose a marine monitoring system that, with the use of a bi-spectrum camera, can detect and estimate the position of boats in different weather and light conditions. We begin our paper by presenting existing vision based monitoring solutions and address their problems in Section 2. This is followed by an explanation of our hardware setup and image calibration in Section 3. The boat detection method is described in Section 4 and the position estimation of detected boats is presented in Section 5. Finally, the conclusion and discussion is found in Section 6. The flow of the system is to first acquire images from each sensor, correct them for distortion, and register them. Boats are then detected in each image separately and subsequently fused in order to not determine the position of the same boat twice. Lastly the boats position is estimated utilizing the predicted bounding box positions. The flow of the system is illustrated in the diagram in Figure 1.

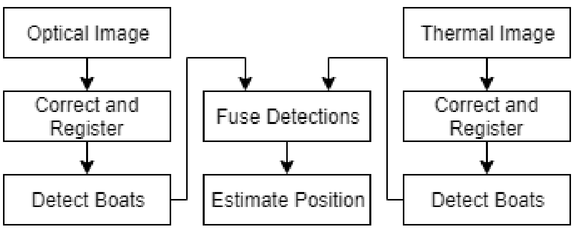

Figure 1: The system flow.

[a] https://orcid.org/0000-0002-1192-9670
[b] https://orcid.org/0000-0001-8235-036X
[c] https://orcid.org/0000-0001-8092-6468
[d] https://orcid.org/0000-0002-8016-2426

The contributions of this paper are as follows:

- We present a boat detection method robust to changing lighting conditions.
- We show that a pretrained Convolutional Neural Network (CNN) based detector can be fine-tuned to the thermal domain using limited training data.
- We propose and evaluate a ray-casting method for positioning boats with a PTZ camera.

2 RELATED WORK

Overview of detection methods: Within the past 20 years, object detection has progressed from traditional detection methods such as Viola Jones Detectors [Viola and Jones, 2001] and HOG Detectors [Dalal and Triggs, 2005], to deep learning detection methods [Zou et al., 2019], predominantly based on the use of convolutional neural networks (CNNs) [Chen et al., 2019] [Zhu et al., 2018]. With the large amounts of annotated data available, as well as accessible GPUs with high computational capabilities, a deep learning era began where object detection started to evolve at an unprecedented speed [Zou et al., 2019] [Liu et al., 2018]. However, there is no universal solution able to solve all detection tasks. This is due to a speed/accuracy trade-off where CNNs that perform faster tend to be less accurate than their more complex and computationally expensive counterparts [Huang et al., 2017]. Two-stage region proposal object detectors such as R-CNNs [Girshick et al., 2013], tend to have great accuracy but require thousands of network evaluations for a single image proving to be computationally expensive [Redmon et al., 2016] [Redmon and Farhadi, 2017]. In contrast, one-stage object detectors such as Single Shot MultiBox Detector [Liu et al., 2016], provide faster detection which comes at the price of accuracy [Huang et al., 2017]. Akiyama et al. proposed a boat detector based on a custom CNN model trained on RGB images from a surveillance camera [Akiyama et al., 2018]. Their model scored an average F1-score of 0.70, but they did not test on any images captured in poor lighting conditions.

Overview of localization methods: Global Positioning System (GPS) localization systems are popular in a plethora of applications [Drawil et al., 2013]. But as previously mentioned smaller vessels are often not equipped with GPS and transponders. Presented with two cameras viewing the same reference point, stereo vision is one method for estimating the position of objects for computer vision applications. This is done by matching images from different viewpoints [Mohan and Ram, 2015]. However, if the cameras operate in different spectra, then depth map based texture matching is difficult to construct, especially with the complexity of the scene. Homography is another method which could be used for localization. The main advantage is a single camera can be used to estimate the position to objects. In this method, the image coordinates are mapped to the coordinates of a known plane [Agarwal et al., 2005]. Yet the problem with this method is that the camera must be fixed in a single position [Agarwal et al., 2005], which would limit the pan and tilt functionality of the PTZ camera. One method often used in video games to determine if and how to render objects, based on the camera's distance and orientation in respect to the object, is ray-casting. This method is applicable using a single camera and allows for camera movement. It requires objects to be defined in 3D space to determine the rays intersection with them and hence evaluate their position in relation to the camera [Hughes et al., 2013].

3 SETUP AND CALIBRATION

The camera used is a Hikvision DS-2TD4166-50[1]. The camera is bi-spectrum with an optical and thermal sensor. The thermal sensor is beneficial as it is independent on external optical light sources and instead utilizes the infrared radiation from objects within the field of view [Gade and Moeslund, 2014]. The Hikvision camera is mounted on a dome, which allows for manipulation of the camera orientation with two degrees of freedom: pan (left/right movement) and tilt (up/down movement). The dome is mounted on top of a building with an overview of a small port, which is visited by everything from cruise ships to kayaks. The camera is connected to a computer with the following specifications: Intel(R) Xeon(R) CPU E5-1620 v4 @ 3.50 GHz, 16.0 GB RAM, Nvidia GeForce GTX 1080 Ti GPU and operating on Windows 10 (64-bit). Both the optical and thermal sensor information will be used in order to create a system which is more robust to environmental conditions. Therefore, the output of the system will be based on a late-fusion of the information of the two sensors. To allow fusion of the sensor information, the images must be registered to the same image plane. Firstly, the intrinsic parameters of the two sensors are calibrated separately. Secondly, the images are aligned by performing image registration. The calibration of the cameras was done using a checkerboard and Zhang's method [Zhang, 2000]. Detecting

[1]Specification list found at [Hikvision, 2019]

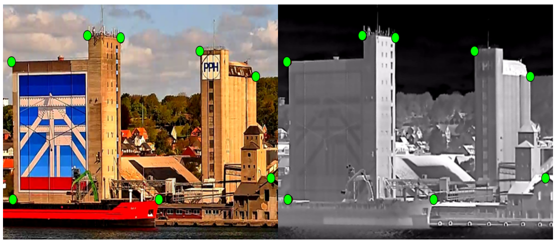

(a) Optical image. (b) Thermal image.

Figure 2: An example of potential feature points indicated by the green circles.

the checkerboard using an optical sensor is straightforward, however, since the thermal sensor captures temperature differences instead of colours, in many conditions a regular checkerboard may seem uniform to the thermal camera. Yet since the calibration was done outside the light from the sun would heat the black tiles more than the white tiles and an inverse version of the checkerboard was visible. The issue of calibrating thermal cameras and different solutions are discussed in [Gade and Moeslund, 2014]. The solution for our system is similar to the one presented in [John et al., 2016]. After correcting the images for potential distortion, they can be registered. The optical image will be registered onto the thermal image. This is done since the thermal sensor has a fixed focal length with a known value which will be desirable for later boat position estimation. The images were registered by performing an affine transformation on the optical image. In order to determine the transformation, a feature based approach was used [Goshtasby, 1988] [Goshtasby, 1986]. In this approach several corresponding feature points are selected manually from both images. The feature points chosen were points such as roof tops and chimneys since these where clearly visible in both images and the points were chosen to span as much of the images as possible. Figure 2 shows feature points in the two images.

4 DETECTOR

For this work, we need the system to perform boat detection in two individual video streams at real time. Furthermore, as small ports and the surrounding waters may experience fast moving boats, like motorboats, the system should run at a high enough frame rate to provide smooth localizations of all boats. This suggests the use of a one stage CNN detector. The one stage object detector chosen was YOLO (You Only Look Once) [Redmon and Farhadi, 2018]. The details will be described in the following section.

4.1 Implementation

There are various implementations of YOLO, each with varying architectures and trained on different datasets for unique applications. Recently, YOLO version 3 (YOLOv3) was released which improved not only the speed but also the accuracy of the previous YOLOv2 [Redmon and Farhadi, 2018]. Furthermore, when processing 320×320 images, YOLOv3 runs as accurate as Single Shot MultiBox Detector [Liu et al., 2016], but three times faster [Redmon and Farhadi, 2018]. For the purposes of our system, the YOLOv3 subvariant chosen was the pre-trained YOLOv3-416 model with 416×416 input image size with weights pre-trained on the Common Objects in Context (COCO) Dataset [Lin et al., 2014]. The input image size was chosen to be as great as possible while still maintaining a high frame rate application. The COCO dataset was chosen as it already has a 'boat' class. Henceforth, when YOLOv3 is mentioned throughout this paper, it refers to the YOLOv3-416 model. With the pre-trained YOLOv3 model, a preliminary performance evaluation on both optical and thermal images of boats was done.

4.1.1 Preliminary Evaluation

To evaluate the performance of the pre-trained YOLOv3 model, the COCO metrics will be calculated. Specifically Average Precision (AP) which is calculated by combining the metrics "precision", "recall" and "Intersection over Union" into a single quantity as shown in [Zhang and Zhang, 2009], where the greater the metric, the better the model. AP is calculated for a single class whereas mean Average Precision (mAP) is calculated by taking the mean of all APs from all classes. In order to evaluate pre-trained YOLOv3's performance on our setup we collected data from our setup manually saving both the optical and thermal image whenever a boat was seen. This resulted in two separate datasets, one for optical images and one for the thermal counterpart, where a small subset of each can be seen in Figure 3. The red boxes in Figure 3 indicate the ground truth bounding box positions of the boats. 288 images for each modality were collected. Following the evaluation metrics set by COCO, the AP was calculated with an IoU threshold of 50% and precision and recall were calculated with a confidence threshold of 25%. Using the testing dataset for optical images resulted in an AP score of 75.58% for boats. An example of running YOLOv3 on the optical images can be seen in Figure 3a, indicated by the green boxes. Using the testing dataset for thermal images resulted in an AP score of 36.42% for boats. This lesser result, compared to the optical data, is to be expected as YOLOv3 is trained using the COCO dataset which is composed solely of optical images and not thermal images. An example of running YOLOv3 on the thermal images can be seen in Figure 3b. To better adapt the detector to the thermal domain, YOLOv3 should be retrained with a set of thermal images. Furthermore, although pre-trained YOLOv3 on optical images had and AP score of 75.58%, it will also be retrained in order to further improve it.

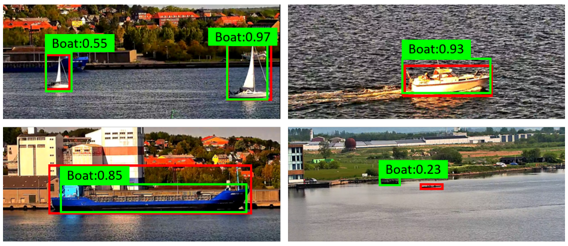

(a) Optical images as input.

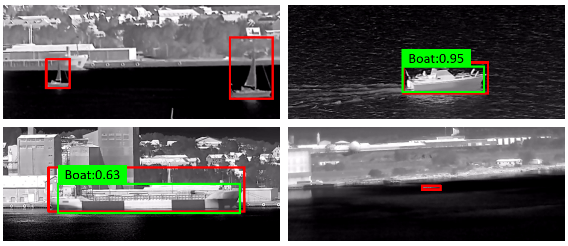

(b) Thermal image as input.

Figure 3: Output of the YOLOv3 model pretrained on the COCO dataset. The red boxes are the ground truth annotations, while the green boxes are the detections.

4.2 Retraining YOLO

In order to retrain a YOLOv3 model for each modality, more data was collected. This resulted in 640 pairs of images, in addition to the preliminary test dataset of 288 images. With these small datasets, transfer learning is utilized in order to avoid retraining the entire model, which requires large amounts of data. When performing transfer learning, certain layers of the model are frozen, where a frozen layer does not change weights during the training process. The rule of thumb is that the more data available, the less layers should be frozen [Yosinski et al., 2014]. As our datasets are limited, it is suggested to freeze the entire feature extractor of the object detector in order to avoid overfitting when training the models [Yosinski et al., 2014]. This is also known as fine-tuning the model. This is the approach taken for the purposes of retraining YOLOv3. We retrain the YOLOv3 network to detect only a single class: ”boat”.

4.2.1 Training

We trained YOLOv3 with an approximately 70/30 (450 and 190 images) split between training data and validation data. The split was done to ensure that the validation dataset contained boats not present in the training dataset. To determine when to stop training each model, the evaluation metrics AP and loss error were used. The loss error is the output from the cost function of the model where the lower the error, the better the model. Hence, training should be stopped at the greatest AP and lowest loss error. A maximum AP of 98% and 97% were reached for the optical and thermal models, respectively, where no further significant decrease in loss was observed.

4.2.2 Evaluation

In order to evaluate the two retrained YOLOv3 models for optical and thermal images, the same evaluation metrics and dataset from the preliminary evaluation in Section 4.1.1 was used. The fine-tuned optical YOLOv3 model had an AP of 95.53% whereas the YOLOv3 model pretrained on the COCO dataset scored an AP of 75.58%. The fine-tuned thermal YOLOv3 model scored an AP of 96.82%, which is a significant increase compared to the model pretrained on the COCO dataset, which scored an AP of 36.42% on the thermal data. The AP scores were calculated with an IoU threshold of 50%. The average IoU was also measured as it gives an indication of how precise the position of the boats can be estimated. The average IoU was 72.36% and 74.14% for the optical and thermal model, respectively. Figure 4 and 5 show some qualitative results on optical and thermal images, respectively.

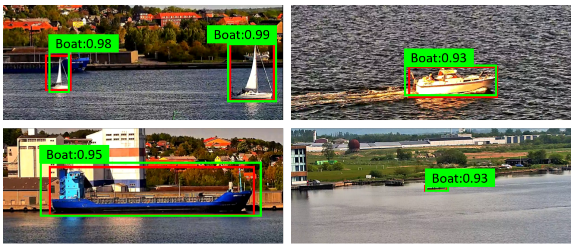

Figure 4: Output of retrained YOLOv3 on optical images

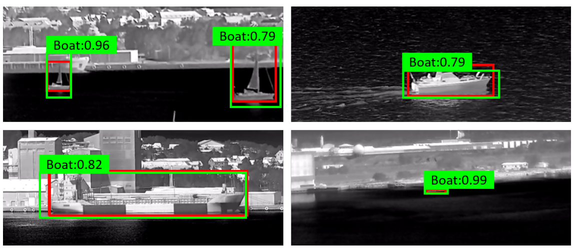

Figure 5: Output of retrained YOLOv3 on thermal images

4.3 Poor Optical Lighting Test

A test was conducted to compare the performance of the models in poor lighting conditions. A dataset was collected containing 24 pairs of images of boats during the night. This dataset is rather small since only a few boats were present during the night. The night dataset was processed by the two fine-tuned models scoring an AP of 15.05% and 46.05% for the optical and thermal model, respectively. Both scores are lower than the evaluation with images captured during daytime but it is clear that the thermal model is outperforming the optical model under low optical light conditions. Examples of processed night images are presented in Figure 6 and Figure 7, where the red boxes indicate the ground truth and the green boxes indicate the model predictions.

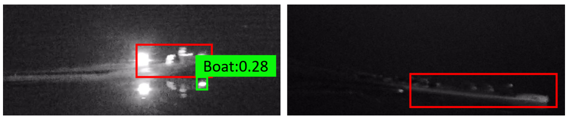

Figure 6: Output of retrained YOLOv3 on the optical image taken during the nights.

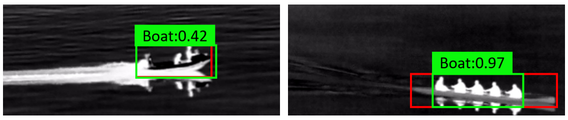

Figure 7: Output of retrained YOLOv3 on the thermal images taken during the nights.

5 POSITION ESTIMATION

The position estimation method chosen for this work is based on the concept of ray-casting, which will be outlined in the following section.

5.1 Ray-Casting Concept

The concept is to cast a ray from a point, representing the boat in either the optical or thermal image, through the focal point of the camera and then determine where this line intersects with a plane, representing the ground [Hughes et al., 2013]. This ray-plane intersection point is then correlated to a position on a map of the harbor providing an estimation of the boat's position. This method will limit the position estimation to the ground coordinates and will not provide the objects height above the ground. This is still applicable for boat detection since the boats will always be placed in the water and the ground plane can therefore be defined as the water level. The position of a detected boat is defined by the lowest center point of the estimated bounding box, as illustrated in Figure 8. This point is expected to be a good estimation of where the center of the boat intersects with the water.

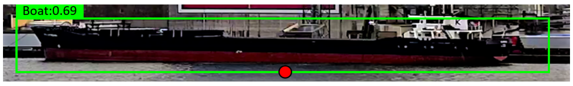

Figure 8: Boat detection indicated by the green bounding box. The red point represents the estimated position of the boat.

5.2 Translating from Pixel to World Coordinates

The estimated position of the boat should now be translated from image to world coordinates. Initially the pixel coordinates are transformed into normalized device coordinates (NDC) and then into sensor coordinates. The sensor coordinate of the image point and the focal point are then defined in respect to the camera's point of rotation in order to introduce the camera orientation. This is done by adding a third dimension to the image point and focal point equal to the point's distance from the point of rotation. The sensor, focal point, and point of rotation are shown in Figure 9.

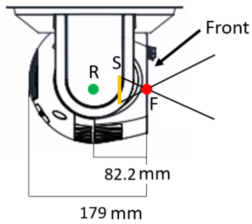

Figure 9: Profile view of the camera. F is the estimated focal point position, S is the estimated sensor position and R is the estimated point of rotation.

The distance between the point of rotation to the focal point and sensor are 82.2 mm and 32.2 mm, respectively. The points can then be rotated around the point of rotation by multiplying them with a rotation matrix incorporating both pan and tilt. The sensor point and focal point are then projected to world space by adding the world position of the camera. This position was set to be $[0,0,22.457]^T$ which defines the cameras x and y position as the world origin and its z position as the cameras height above the water surface. A potential issue here is that the water level might change due to tides which will alter the distance between the camera and water surface. However, this is assumed to be of minor significance and is therefore not further investigated.

5.3 Ray-Plane Intersection

Now that the sensor point and focal point have been defined in world space, a ray can be cast from the sensor point, through the focal point and the ray's intersection with the ground plane as described in [Hughes et al., 2013]. This is done by first calculating the solution parameter given by

$$s_i = \frac{\mathbf{n} \cdot (V - P0)}{\mathbf{n} \cdot (P1 - P0)}, \quad (1)$$

where $\mathbf{n}$ is the plane normal vector, V is an arbitrary point on the plane, and $P0$ and $P1$ are the sensor point and focal point defining the ray. For this system $\mathbf{n} = [0,0,1]^T$ and $V = [0,0,0]^T$.

The intersection can then be calculated by

$$P(s_i) = P0 + s_i \cdot (P1 - P0), \quad (2)$$

where $P(s_i)$ is the ray-plane intersection. Finally, the position is correlated with a map, scaled such that one pixel equals one meter in the world, and the position of the camera is added as an offset to the boat's estimated position.

5.4 Fusing Detections

Lastly, an algorithm was created to fuse the detections from the two detectors. This was done in order to only calculate one position of the boat, even if it is detected by both sensors. This is done by determining the IoU between the detections in the thermal image and the detections in the optical image. If the IoU is above a threshold of 0.5 it is determined that the detection by the thermal detector is also detected by the optical detector and only the position of the optical detection is estimated. Otherwise, a position will be estimated based on the individual detections from the sensors. The estimated position can now be correlated with a satellite map of the world. This map can be seen in Figure 12. The map was scaled so that 1 pixel in the map corresponds to 1 meter in the world.

5.5 Calibration

The orientation of the camera was aligned with the orientation of the map by offsetting the tilt and pan of the camera. The estimated position of the waterfront's intersection with the waterline was tested. This test showed that estimated position started to deviate from the true position as the camera was panned to the right, illustrated in Figure 10. In this image the green line indicates the line on which the positions should lie and the dotted red line illustrate where they actually lay. This error was expected to be because of panoramic distortion which is a mechanical effect which cause straight lines to curve as the camera is panned [Luhmann, 2008]. This expectation was

Figure 10: An illustration of a problem with the position estimation when panning to the right. The dotted red line is the position given by the estimator and the green line is the actual position of the waterfront.

tested by creating a panoramic image of the waterfront which can be seen in Figure 11. In this image the green line indicates the expected direction of the waterfront if no distortion is present and the red dotted line indicates the actual shape of the waterfront in the images. The panoramic image was created manually by connecting images in succession and no other manipulation of the images was performed. Comparing Figure 10 and 11 the estimation error follows the panoramic distortion well. The error was mitigated by applying a function to the tilt based on a fraction of the pan angle given by

$$t = t + (\frac{p}{f}), \quad (3)$$

where t and p are tilt and pan respectively and f is the fraction. The equation is only applied when the pan angle is negative, i.e., where the camera is pointing to the right, since this was the side that produced the error. The fraction of the pan angle was found through empirical tests.

5.6 Evaluation

In order to evaluate the position estimator, points recognizable in both the image and on the map were used. This resulted in the points on the waterfront shown in Figure 12, where the circles represent the chosen position, the stars represent the estimated position, and the colors indicate the connection between points. The yellow line is added to clarify the connection and show by how much they differ. Since the points which are recognizable in both the images and on the map only lie on the edges of the waterfront, and not on the water, an additional test was performed. In this test the position of a boat on the water was estimated over time. Simultaneously the boat's GPS position was recorded from a boat tracking website [MarineTraffic, 2019] which was used as ground truth. The position of the boat detected by both systems is plotted in Figure 12 as the points on the water, in which the triangles represent the estimated position and the connected circles represent the position from the tracking software. The mean and standard

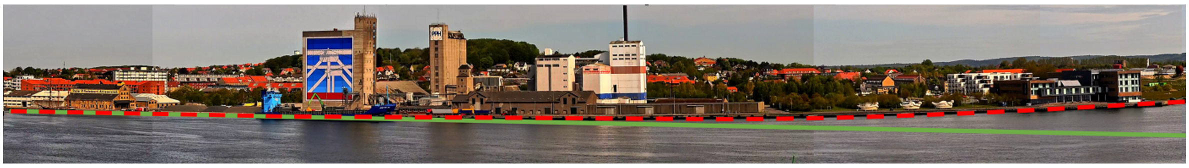

Figure 11: A panoramic image created of the waterfront. The dotted red line showing the waterfront as seen by the camera and the green line indicating the expected shape of the waterfront provided no panoramic distortion.

Figure 12: Position estimation test results. Circles represent the true position. Stars and triangles represent the estimated position.

deviation error of the position estimator for the points on the waterfront where 12.54m and 11.49m respectively, 25.63m and 21.30m for the tracked boat and, 18.58m and 19.87m when the two where combined. The reason for the mean and standard deviation being higher for the boat points. The reason for the mean and standard deviation being higher for the boat positions is most likely due to the inaccuracy of the embedded GPS systems which, by the International Maritime Organization (IMO), are expected to be around 10 meters [IMO, 2001].

6 CONCLUSION

In this paper we present a method for monitoring boat traffic in ports using computer vision. The proposed method is divided into subsystems, which were tested separately. The detection accuracy of YOLOv3 was increased from an AP score of 75.58% and 36.42% for optical and thermal images, respectively, to 95.53% and 96.82% when fine-tuned with just 450 annotated images. When testing models with a dataset of images during low optical light conditions the thermal model outperforms the optical model as expected. The AP scores were 15.05% and 46.05%, for the optical and thermal model, respectively. The position estimation was evaluated to have a mean error between 12.54 m and 25.63 m depending on the location of the estimated point. A large error was generally experienced when estimating positions of boats, which was most likely caused by inaccurate GPS positions used as ground truth. Combining all subsystems we have shown that boat traffic at ports can be monitored by a single bi-spectrum camera. We have shown that YOLOv3 can be retrained to detect boats in optical and thermal images using a limited amount of data. Lastly, we have shown that the position of boats can be estimated using ray-casting.

6.1 DISCUSSION

The boat detector is run twice: once for the optical image and once for the thermal. A solution that would simplify and speed up the system would be to incorporate early fusion, where the optical image and thermal image are combined to create a 4-channel image and run only a single instance of object detection. However, that would require that the network is designed for 4-channel images, and trained with a large amount of 4-channel data. The test in low optical light conditions should also be redone with a larger dataset to get a better sense of the performance difference between the two detectors. Both models could likely also be improved for detecting boats during low optical lighting conditions by training them with data captured in low optical lighting. The position estimator could be improved by creating a better model for correction the panoramic distortion along with a better calibration of the setup. A sensor constantly monitoring the water level could also be implemented to more precisely determine the cameras height above the water. The position estimator should ideally be tested using more accurate ground truth data. A tracking algorithm could also be implemented for the purpose of tracking the detected boats in the images. This would ease the needed computations since the object detector would not need to be run for each frame. This tracker could also provide more information such as the path of certain boats and their velocity. An additional advantage of tracking would be the ability to automatically pan and tilt the camera to follow a specific boat. Classifying detected boats would be beneficial in order to gain further statistical data about the boats entering and leaving ports. This could be done, provided enough data, by retraining both detection models to detect particular types of boats such as sailboats, motorboats, and tankers.

REFERENCES

Agarwal, A., Jawahar, C. V., and Narayanan, P. J. (2005). A survey of planar homography estimation techniques. Technical report.

Akiyama, T., Kobayashi, Y., Kishigami, J., and Muto, K. (2018). Cnn-based boat detection model for alert system using surveillance video camera. In *2018 IEEE 7th Global Conference on Consumer Electronics (GCCE)*, pages 669–670.

Branch, A. E. (1986). *Port traffic control*, pages 124–143. Springer Netherlands, Dordrecht.

Chen, K., Pang, J., Wang, J., Xiong, Y., Li, X., Sun, S., Feng, W., Liu, Z., Shi, J., Ouyang, W., Loy, C. C., and Lin, D. (2019). Hybrid task cascade for instance segmentation.

Council of the European Union (2008). Maritime surveillance - overview of ongoing activities. Technical report, European Union, Brussels.

Dalal, N. and Triggs, B. (2005). Histograms of oriented gradients for human detection. In *2005 IEEE Computer Society Conference on Computer Vision and Pattern Recognition (CVPR'05)*, volume 1, pages 886–893 vol. 1.

Drawil, N., Amar, H., and Basir, O. (2013). Gps localization accuracy classification: A context-based approach. *Intelligent Transportation Systems, IEEE Transactions on*, 14:262–273.

Gade, R. and Moeslund, T. (2014). Thermal cameras and applications: A survey. *Machine Vision and Applications*, 25:245–262.

Girshick, R., Donahue, J., Darrell, T., and Malik, J. (2013). Rich feature hierarchies for accurate object detection and semantic segmentation.

Goshtasby, A. (1986). Piecewise linear mapping functions for image registration. *Pattern Recognition*, 19(6):459 – 466.

Goshtasby, A. (1988). Image registration by local approximation methods. *Image and Vision Computing*, 6(4):255 – 261.

Hikvision (2019). Ds-2td4166-25(50). https://www.hikvision.com/en/Products/Thermal-Camera/Network-Speed-Dome/640512-Series/DS-2TD4166-25(50).

Huang, J., Rathod, V., Chen, S., Zhu, M., Korattikara, A., Fathi, A., Fischer, I., Wojna, Z., Yang, S., Guadarrama, S., and Murphy, K. (2017). Speed/accuracy trade-offs for modern convolutional object detectors.

Hughes, J. F., van Dam, A., McGuire, M., Sklar, D. F., Foley, J. D., Feiner, S. K., and Akeley, K. (2013). *Computer graphics: principles and practice (3rd ed.)*. Addison-Wesley Professional, Boston, MA, USA.

IMO (2001). Guidelines for the onboard operational use of shipborne automatic identification systems (ais). page 6.

John, V., Tsuchizawa, S., Liu, Z., and Mita, S. (2016). Fusion of thermal and visible cameras for the application of pedestrian detection. *Signal Image and Video Processing*.

Lin, T., Maire, M., Belongie, S. J., Bourdev, L. D., Girshick, R. B., Hays, J., Perona, P., Ramanan, D., Dollár, P., and Zitnick, C. L. (2014). Microsoft COCO: common objects in context. *CoRR*, abs/1405.0312.

Liu, L., Ouyang, W., Wang, X., Fieguth, P., Chen, J., Liu, X., and Pietikäinen, M. (2018). Deep Learning for Generic Object Detection: A Survey. *arXiv e-prints*, page arXiv:1809.02165.

Liu, W., Anguelov, D., Erhan, D., Szegedy, C., Reed, S., Fu, C.-Y., and Berg, A. C. (2016). Ssd: Single shot multibox detector. *Lecture Notes in Computer Science*, page 2137.

Luhmann, T. (2008). A historical review on panorama photogrammetry. *International Archives of the Photogrammetry, Remote Sensing and Spatial Information Sciences*, 34.

MarineTraffic (2019). Marinetraffic: Global ship tracking intelligence — ais marine traffic. https://www.marinetraffic.com/.

Mohan, D. and Ram, D. A. R. (2015). A review on depth estimation for computer vision applications. volume 4.

Redmon, J., Divvala, S., Girshick, R., and Farhadi, A. (2016). You only look once: Unified, real-time object detection. pages 779–788.

Redmon, J. and Farhadi, A. (2017). Yolo9000: Better, faster, stronger. *2017 IEEE Conference on Computer Vision and Pattern Recognition (CVPR)*, pages 6517–6525.

Redmon, J. and Farhadi, A. (2018). Yolov3: An incremental improvement. *CoRR*, abs/1804.02767.

Viola, P. and Jones, M. (2001). Rapid object detection using a boosted cascade of simple features. In *Proceedings of the 2001 IEEE Computer Society Conference on Computer Vision and Pattern Recognition. CVPR 2001*, volume 1, pages I–I.

Wiersma, E. and Mastenbroek, N. (1998). Measurement of vessel traffic service operator performance. *AI & SOCIETY*, 12(1):78–86.

Yosinski, J., Clune, J., Bengio, Y., and Lipson, H. (2014). How transferable are features in deep neural networks. *CoRR*, abs/1411.1792.

Zhang, E. and Zhang, Y. (2009). *Average Precision*, pages 192–193. Springer US, Boston, MA.

Zhang, Z. (2000). A flexible new technique for camera calibration. *IEEE Transactions on Pattern Analysis and Machine Intelligence*, 22(11):1330–1334.

Zhu, R., Zhang, S., Wang, X., Wen, L., Shi, H., Bo, L., and Mei, T. (2018). Scratchdet: Training single-shot object detectors from scratch.

Zou, Z., Shi, Z., Guo, Y., and Ye, J. (2019). Object detection in 20 years: A survey. *CoRR*, abs/1905.05055.